JOM, Vol. 69, No. 7, 2017
DOI: 10.1007/s11837-017-2365-z

Metallic Glass Nano-composite Thin Films for High-performance Functional Applications

SANTANU DAS,[1,3] HARPREET SINGH ARORA,[1,2] and SUNDEEP MUKHERJEE[1,4]

1.—Department of Materials Science and Engineering, University of North Texas, Denton, TX 76203, USA. 2.—Department of Mechanical Engineering, Shiv Nadar University, Gautam Buddha Nagar, Uttar Pradesh 201314, India. 3.—*Present address:* Department of Ceramic Engineering, Indian Institute of Technology (BHU), Varanasi, Uttar Pradesh 221005, India. 4.—e-mail: Sundeep.Mukherjee@unt.edu

Metallic glass nanocomposite thin films were synthesized for an immiscible Ag-Cu alloy system by magnetron sputtering. The structure of the films was unique, consisting of homogeneously dispersed nanocrystallites in an amorphous matrix. The size and volume fraction of the nanocrystallites increased with increasing film thickness resulting in increased elastic modulus and hardness. The high electrical conductivity of the nanocomposite films was examined by a valence-band study, which showed that exchange interaction between Ag and Cu in the nanocomposite structure resulted in enhanced charge carrier concentration. The inverse correlation between electrical conductivity and film thickness was explained by surface and interface scattering of electrons with increasing volume fraction of nanocrystallites. The small temperature dependence of conductivity was attributed to the distorted Fermi surface of the nanocomposite films resulting in a greater contribution from structure scattering, which is temperature-independent.

INTRODUCTION

Individually, silver (Ag) and copper (Cu) exhibit the highest electrical conductivity among metals and are widely used for numerous scientific and industrial applications. However, Ag and Cu are mutually immiscible due to their positive heat of mixing.[1] In an immiscible system, the mixing of the constituent elements even in the liquid state may be unfavorable,[2,3] and long-range chemical partitioning may be suppressed by quenching or other non-equilibrium processing. However, some degree of energy minimization results in the development of local structures on extremely fine scales.[4] Formation and stabilization of amorphous phases in immiscible systems have also been reported,[5,6] along with a strong clustering tendency leading to non-uniform spinodal-like structures.[5] Vapor deposition and other far-from-equilibrium processing techniques may be employed to extend solid solubility in immiscible systems.[5–13] Sputtering represents a versatile technique for producing homogeneous thin films of immiscible alloys with varying composition and tunable properties.[14,15] While there are a few studies on the structure as a function of composition for silver-copper alloys by far-from-equilibrium processing,[13,16–18] there are no reports on the physics of electrical transport in this immiscible system of immense technological importance. Fundamental understanding of electrical transport properties in Ag-Cu alloys has the potential to open up a new paradigm of highly conducting metals for deeply scaled interconnects, energy conversion technologies, and micro-/nano-electromechanical systems (MEMS/NEMS).

Here, we demonstrate a highly conductive nanocrystallite dispersed amorphous structure synthesized from an immiscible Ag-Cu alloy system. Nanocomposite films of nominal composition ~60 at.% Ag–40 at.% Cu were synthesized by direct current (DC) magnetron sputtering. This particular composition was chosen because it is close to a eutectic and therefore glass formation is likely to be favored. The structure of the nanocomposite films was unique, consisting of homogeneously dispersed nanocrystallites in an amorphous matrix. The size

(Published online April 28, 2017)

and volume fraction of the nanocrystallites increased with increasing film thickness resulting in increased elastic modulus and hardness. These nanocomposite films showed high electrical conductivity, with a very small temperature dependence. The high conductivity of the nanocomposite films was attributed to the d–d band interaction of Ag and Cu, leading to an increased density of charge carriers as seen from their valence band structure.

EXPERIMENTAL

Nanocomposite Ag-Cu thin films of composition 60.1 at.% Ag–39.9 at.% Cu were sputter-deposited onto thermal oxide-grown (thickness of ~300 nm) Si substrates. Three different film thicknesses of 50 nm, 100 nm, and 200 nm were deposited by varying deposition time at a constant deposition rate (1.39 Å/s). Substrate temperature during the deposition processes was kept at around 16°C. A 2-nm coating of Cr was used to ensure good film-substrate adhesion. The film thicknesses were measured using a profilometer (Vecco, USA) to be: 50 nm ± 1.6 nm, 100 nm ± 4.9 nm, and 200 nm ± 11.1 nm, respectively. More experimental details and characterization of the thin ilms are discussed in the supplementary information Section S1.

RESULTS AND DISCUSSION

Figures S1a and S1b (supplementary information) show the characteristic Cu 2*p* and Ag 3*d* peaks measured using XPS for the 50-nm-thick film. Similar peak positions were also obtained for the 100-nm- and 200-nm-thick films. The energy difference (i.e. core-level spin orbital splitting) between $3d_{5/2}$ and $3d_{3/2}$ for Ag (6.0 eV) as well as between $2p_{3/2}$ and $2p_{1/2}$ for Cu (19.8 eV) were found to be unchanged, which shows the metallic states of the respective elements in the nanocomposite films. However, a slight shift of the Ag $3d_{5/2}$ peak to higher binding energy and a slight shift of the Cu $2p_{3/2}$ peak to lower binding energy may be attributed to nearest neighbors of different kinds in the alloy, in contrast to pure metals. After baseline correction followed by XPS peak fitting, the composition of each nanocomposite film (10-point average) was calculated to be: Ag ~60 at.% ± 0.4 at.%, Cu 39.7 at.% ± 0.28 at.%, and 0.3% others. This suggests no surface segregation of either Cu or Ag in the alloy.

The structure of the nanocomposite films of different thicknesses was investigated using transmission electron microscopy. Figure 1 shows the HRTEM images of 50 nm, 100 nm, and 200 nm nanocomposite films. It is clearly seen that nanocrystallites of various sizes are uniformly dispersed in an amorphous matrix. The corresponding SAED patterns are illustrated in Fig. 1d, e, and f for 50 nm, 100 nm, and 200 nm films, respectively. The size of the nanocrystallites varies from 1 nm to 10 nm for 50-nm-thick film. Figure 1b shows the HRTEM image of the 100-nm nanocomposite film with homogeneously dispersed nanocrystallites in an amorphous matrix. Figure 1e shows the corresponding SAED pattern with small dots inside the diffuse diffraction rings, which is representative of the nanocomposite structure. Figure 1c shows the HRTEM image of the 200-nm film with comparatively larger nanocrystallite size as well as larger volume fraction. This was further confirmed from the SAED pattern shown in Fig. 1f. Several multifaceted, overlapping, and twinned regions were found in the 200-nm film, which is attributed to stress and thickness distribution.

Figure S2 (supplementary information) shows the variation of the nanocrystallite volume fraction in the films with different thicknesses. For the 50-nm-thick film, ~80% of the nanocrystallites were in the size range of 3–6 nm, which further increased to ~93% in the 100-nm film. The size distribution of the nanocrystallites suggests that the number of nucleated sites increased in nanocomposite films goes from 50 nm to 100 nm, while these nuclei grow upon a further increase of film thickness to 200 nm (Figure S3, supplementary information). The increase in size and volume fraction of the nanocrystallites (Figure S2, supplementary information) suggests that the rate of *quenching* varies with the thickness of the film, and is proportional to the rate of heat dissipation from the film to the substrate.[14] The kinetic constraint decreases with increasing film thickness, resulting in a larger fraction of nanocrystallites. Phase separation behavior has recently been reported for Ag-Cu alloy nanoparticles grown by DC magnetron sputtering and found to be composition- and crystallite size-dependent.[19] Particles below 5 nm diameter were found to grow as a Ag-Cu solid solution for compositions of 15–80 at.% Ag. For higher Ag content of 60–80 at.%, no phase separation was observed until about 10-nm particle size. The critical size for phase separation was connected to the critical wavelength for fast-growing concentration fluctuations and the instability of the solid solution state.[19] In the current study on 60 at.% Ag, the majority of the nano-crystallites were found to be in the size range below 10 nm for all three film thicknesses. Therefore, the nanocrystallites are likely to be single-phase solid solutions with no phase separation.

The structure of the thin films and the corresponding sputtering target were analyzed by XRD as shown in Fig. 2. The increase in nanocrystallite size and volume fraction with increasing film thickness are also evident from the XRD patterns. For the 50-nm film, the XRD pattern shows a broad hump, indicating that the structure is almost entirely amorphous. However, with increasing film thickness, the XRD patterns for the 100-nm and 200-nm films show a decreasing trend for full-width half-maxima, suggesting nucleation of crystalline phases in the amorphous matrix.[20,21] XRD characterization of the binary-alloy (60.12 at.% Ag–

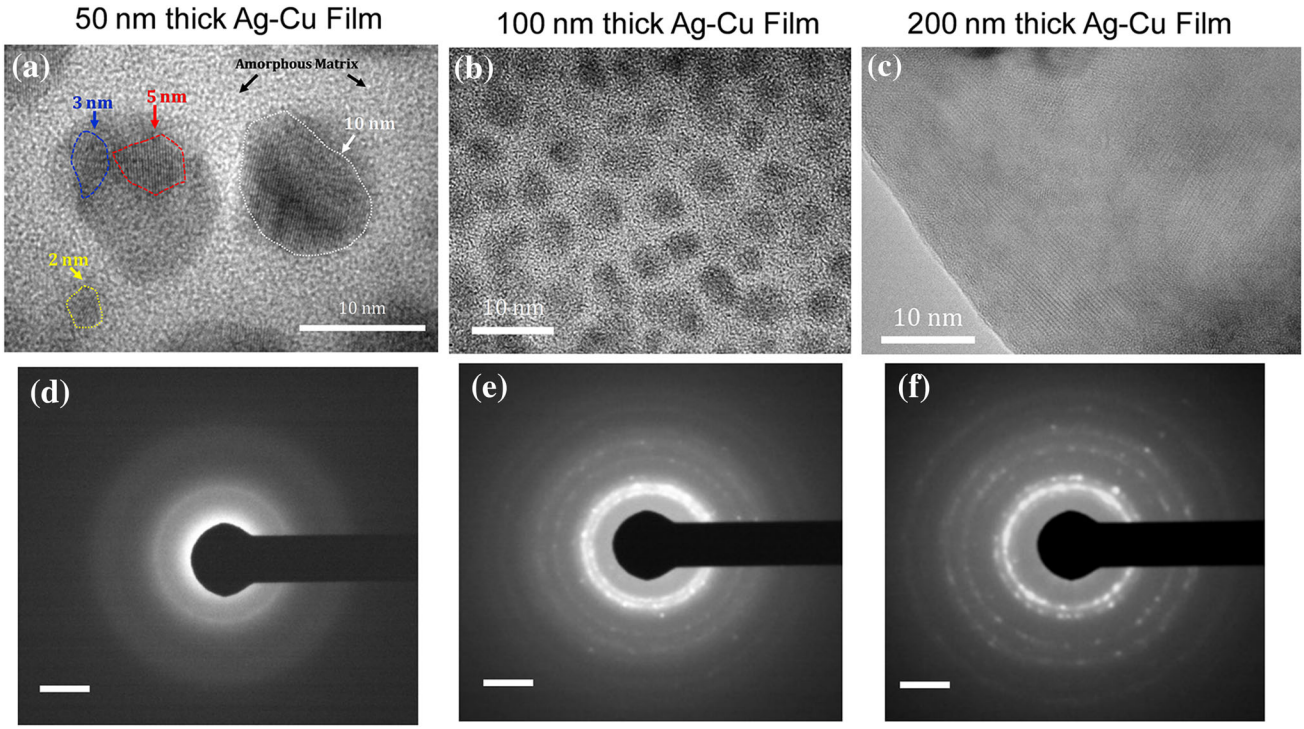

Fig. 1. HRTEM images of nanocomposite films of thicknesses of (a) 50 nm, (b) 100 nm, and (c) 200 nm; selected area electron diffraction pattern of nanocomposite films of thicknesses of (d) 50 nm, (e) 100 nm, and (f) 200 nm. Scale bars 10 nm.

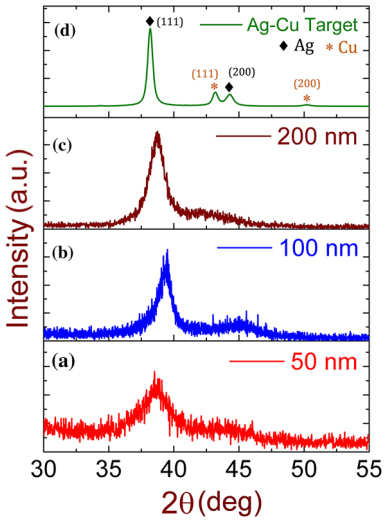

Fig. 2. X-ray diffraction pattern for Ag-Cu nanocomposite films of thicknesses of (a) 50 nm, (b) 100 nm, and (c) 200 nm; (d) XRD of Ag-Cu sputtering target showing peaks corresponding to pure Ag and pure Cu.

39.88 at.% Cu) sputtering target was also carried out (Fig. 2d). The XRD pattern shows a clear signature of pure Ag and pure Cu peaks, indicative of an immiscible binary eutectic alloy.

Nanomechanical characteristics of the composite films of thickness 50 nm, 100 nm, and 200 nm were evaluated by nano-indentation. Figure 3a and b shows the variation in elastic modulus and hardness as a function of film thickness, respectively. Both the modulus and hardness increase with increasing thickness, which is attributed to the increasing crystallite volume fraction. Electrical conductivity of the nanocomposite films was measured using the four-point probe technique and the data are shown in Fig. 3c. Electrical conductivities measured as a function of temperature for all the nanocomposite films are shown in Fig. 3d. Figure 3c shows that the 50-nm film has a high electrical conductivity $\sim 5.09 \times 10^5 \pm 2.93 \times 10^4$ S cm^{-1}, close to single-crystal Ag.[22] The conductivity decreased with increasing film thickness to 100 nm and further to 200 nm. This may be attributed to increased phonon scattering with the increase in fraction of the nanocrystalline/amorphous interfaces.[23,24] Conductivity was also measured as a function of temperature (Fig. 3d) over the range of 77–340 K, and the nanocomposite films exhibited very small temperature dependence. Electrical resistivity has contributions from thermal scattering as well as structure scattering.[25,26] In the nanocomposite films, the Fermi surface is likely to be highly distorted, resulting in a greater contribution to resistivity from structure scattering, which is temperature-independent. This supports the small temperature dependence of conductivity seen for all the Ag-Cu nanocomposite films.[25–28]

Figure 4 shows the valence bands of the nanocomposite films characterized by ultra-violet photoemission spectroscopy (UPS). Alongside are shown the spectra for 99.99% Cu and the 99.99% Ag films under

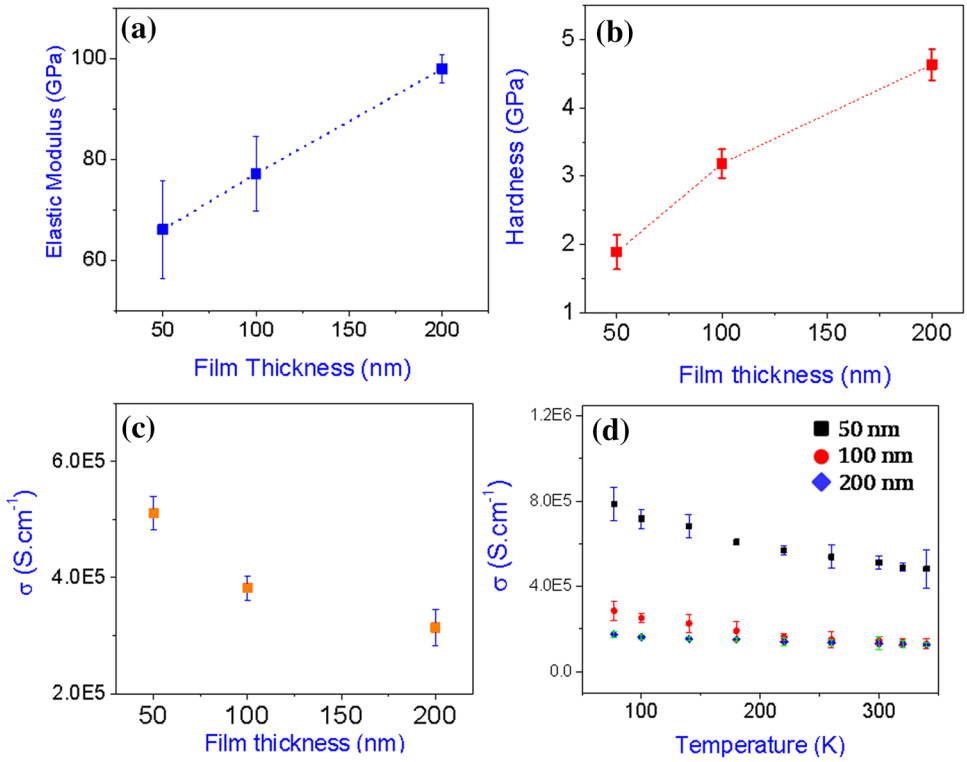

Fig. 3. (a) Elastic modulus and (b) hardness of Ag-Cu nanocomposite films as a function of film thickness; (c) room-temperature electrical conductivity as a function of nanocomposite film thickness; (d) temperature dependence of electrical conductivity for Ag-Cu nanocomposite films of thickness 50 nm, 100 nm, and 200 nm.

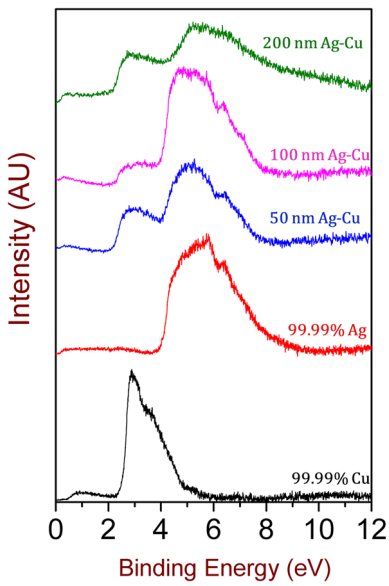

Fig. 4. UPS spectra illustrating the valence band of nanocomposite films of different thicknesses as well as pure elemental Ag and Cu (purity 99.99%).

identical experimental conditions. The broad UPS peaks for pure Cu (electron configuration: [Ar] $3d^{10}$ $4s^1$) and pure Ag (electron configuration: [Kr] $4d^{10}$ $5s^1$) correspond to their respective d-bands. The area under the peak is proportional to the density of states.[29] Compared to elemental valence bands of Ag and Cu, the Ag-Cu nanocomposite films of all three thicknesses show two broad peaks with binding energies in a range around pure Ag and pure Cu. Figure 4 shows that both the Cu and Ag d-bands became broader (area increase) in the alloy compared to their respective elemental form. The broader *d*-band of nanocomposite films suggests overlapping exchange interaction between the constituent elements.[30] The wider valence band increases the density of states and creates additional charge carriers for the alloy. Nanocrystallite formation with increasing film thickness suppresses the Cu 3*d*-band edge, which results in conductivity decrease (Fig. 3c).[31] The peaks get further suppressed for the 200-nm film, with both Ag and Cu peaks of comparable intensity. The increased volume fraction of nano-crystallites for the 100-nm and 200-nm films likely results in greater surface and grain boundary scattering of electrons resulting in lower conductivity.[32–35] These scattering events manifest as broadening of Ag and Cu d-band edge with lowering of their peak intensity.

CONCLUSION

High-conductivity nanocrystalline dispersed amorphous thin films were synthesized for a Ag-Cu immiscible binary alloy system. The 50-nm film exhibited high electrical conductivity of 5.09×10^5 S cm^{-1} and

the conductivity decreased with increasing film thickness. The decrease in conductivity with increasing volume fraction of nanocrystallites is attributed to increased surface and grain boundary scattering of electrons. However, all the films exhibited very small temperature dependence of conductivity. Valence band studies showed that interaction between outer d-bands of Ag and Cu resulted in enhanced charge carrier concentration and increased density of states. This study sets the stage for developing high-performance conductors from immiscible systems with outstanding electrical and mechanical properties at a reduced length scale. Possible applications include nano-electromechanical systems (NEMS) and nanomechanical actuators, which demand tailoring of both electrical and mechanical properties.

ACKNOWLEDGEMENT

This work was partly supported by funding from Semiconductor Research Corporation (SRC/CEMPI Task ID: 2071.031). The authors also gratefully acknowledge the Center for Advanced Research and Technology (CART) at UNT for some of the characterization.

ELECTRONIC SUPPLEMENTARY MATERIAL

The online version of this article (doi:10.1007/s11837-017-2365-z) contains supplementary material, which is available to authorized users.

REFERENCES

1. R. Najafabadi, D.J. Srolovitz, E. Ma, and M. Atzmon, *J. Appl. Phys.* 74, 3144 (1993).
2. A. Puthucode, A. Devaraj, S. Nag, S. Bose, P. Ayyub, M.J. Kaufman, and R. Banerjee, *Philos. Mag.* 94, 1622 (2014).
3. R. Banerjee, A. Puthucode, S. Bose, and P. Ayyub, *App. Phys. Lett.* 90, 021904 (2007).
4. E. Ma, *Prog. Mater Sci.* 50, 413 (2005).
5. J.H. He, H.W. Sheng, P.J. Schilling, C.L. Chien, and E. Ma, *Phys. Rev. Lett.* 86, 2826 (2001).
6. J.H. He, H.W. Sheng, and E. Ma, *Appl. Phys. Lett.* 78, 1343 (2001).
7. P. Duwez, R.H. Willens, and W. Klement, *J. App. Phys.* 31, 1136 (1960).
8. R.K. Linde, *J. App. Phys.* 37, 934 (1966).
9. F. Wu, P. Bellon, A.J. Melmed, and T.A. Lusby, *Acta Mater.* 49, 453 (2001).
10. L.C. Wei and R.S. Averback, *J. Appl. Phys.* 81, 613 (1997).
11. B.Y. Tsaur, S.S. Lau, and J.W. Mayer, *Appl. Phys. Lett.* 36, 823 (1980).
12. R. Stoering and H. Conrad, *Acta Metall.* 17, 933 (1969).
13. C.N.J. Wagner, T.B. Light, N.C. Halder, and W.E. Lukens, *J. Appl. Phys.* 39, 3690 (1968).
14. A.C. Rastogi, S.N. Sharma, and S. Kohli, *Semicond. Sci. Technol.* 15, 1011 (2000).
15. I. Atanasov, R. Ferrando, and R.L. Johnston, *J. Phys.: Condens. Matter* 26, 275301 (2014).
16. L.C. Wei and R.S. Averback, *J. Appl. Phys.* 81, 613 (1997).
17. S. Tanasescu, A. Milea, O. Gingu, F. Maxim, C. Hornoiu, S. Preda, and G. Sima, *Phys. Chem. Chem. Phys.* 17, 28322 (2015).
18. S.B. Kushchev, M.A. Bosykh, S.V. Kannykin, A.V. Kostyuchenko, S.A. Soldatenko, and M.S. Antonova, *Inorg. Mater.* 51, 673 (2015).
19. G. Radnoczi, E. Bokanyi, Z. Erdelyi, and F. Misjak, *Acta Mater.* 123, 82 (2017).
20. A. Li, Y. Jin, D. Muggli, D.T. Pierce, H. Aranwela, G.K. Marasinghe, T. Knutson, G. Brockman, and J.X. Zhao, *Nanoscale* 5, 5854 (2013).
21. R.S. Chaliha, K. Annapurna, A. Tarafder, V.S. Tiwari, P.K. Gupta, and B. Karmakar, *Spectrochim. Acta Part A* 75, 243 (2010).
22. J.Y. Kim, M.-W. Oh, S. Lee, Y.C. Cho, J.-H. Yoon, G.W. Lee, C.-R. Cho, C.H. Park, and S.-Y. Jeong, *Sci. Rep.* 4, 5450 (2014).
23. L. Tian, I. Anderson, T. Riedemann, and A. Russell, *Acta Mater.* 77, 151 (2014).
24. H.F. Lee, S. Kumar, and M.A. Haque, *Acta Mater.* 58, 6619 (2010).
25. T.E. Faber and J.M. Ziman, *Philos. Mag.* 11, 153 (1965).
26. J.M. Ziman, *Philos. Mag.* 6, 1013 (1961).
27. A.K. Sinha, B.C. Giessen, and D.E. Polk, *Treatise on Solid State Chemistry*, ed. N.B. Hannay (New York: Springer, 1976), p. 1.
28. A.K. Sinha, *Phys. Rev. B* 1, 4541 (1970).
29. S. Hüfner, G.K. Wertheim, and J.H. Wernick, *Phys. Rev. B* 8, 4511 (1973).
30. F. Satoru, *Jpn. J. Appl. Phys.* 5, 643 (1966).
31. W. Yang, H. Liu, Y. Zhao, A. Inoue, K. Jiang, J. Huo, H. Ling, Q. Li, and B. Shen, *Sci. Rep.* 4, 6233 (2014).
32. K. Fuchs, *Math. Proc. Camb. Philos. Soc.* 34, 100 (1938).
33. A.F. Mayadas, M. Shatzkes, and J.F. Janak, *Appl. Phys. Lett.* 14, 345 (1969).
34. E.H. Sondheimer, *Adv. Phys.* 1, 1 (1952).
35. J.S. Chawla, F. Gstrein, K.P. O'Brien, J.S. Clarke, and D. Gall, *Phys. Rev. B* 84, 235423 (2011).